Mass spectrometry imaging of mating *Tetrahymena* show that changes in cell morphology regulate lipid domain formation

Michael E. Kurczy[a,c], Paul D. Piehowski[a], Craig T. Van Bell[b], Michael L. Heien[a], Nicolas Winograd[a], and Andrew G. Ewing[a,c,1]

[a]Department of Chemistry, Pennsylvania State University, University Park, PA 16802; [b]Department of Biology, Edinboro University, Edinboro PA 16444; and [c]Department of Chemistry, Göteborg University, Kemivägen 10, SE-41296 Göteborg, Sweden

Edited* by Steven Boxer, Stanford University, Stanford, CA, and approved December 28, 2009 (received for review July 20, 2009)

Mass spectrometry imaging has been used here to suggest that changes in membrane structure drive lipid domain formation in mating single-cell organisms. Chemical studies of lipid bilayers in both living and model systems have revealed that chemical composition is coupled to localized membrane structure. However, it is not clear if the lipids that compose the membrane actively modify membrane structure or if structural changes cause heterogeneity in the surface chemistry of the lipid bilayer. We report that time-of-flight secondary ion mass spectrometry images of mating *Tetrahymena thermophila* acquired at various stages during mating demonstrate that lipid domain formation, identified as a decrease in the lamellar lipid phosphatidylcholine, follows rather than precedes structural changes in the membrane. Domains are formed in response to structural changes that occur during cell-to-cell conjugation. This observation has wide implications in all membrane processes.

lipid domains | membranes | phosphatidylcholine

During cellular function, the structure and the chemical composition of the cell membrane is continuously being modified via dynamic fusion and fission events with internal organelles (1). The highly complex lipid composition of membranes plays a significant role in cell function by the construction of membrane features (2, 3) such as pores and lipid domains (4–7). It is not surprising that abnormalities in lipid composition and membrane function have been implicated in a myriad of disorders, ranging from neurological to cardiovascular (8–12). Furthermore, an understanding of specialized membrane features and disease suggests a unique prospect for therapies that directly target lipid molecules and lipid domains (12).

The *Tetrahymena* model of membrane fusion is ideal to study temporal changes in lipid dynamics related to lipid composition. Complementary mating *Tetrahymena* fuse and then form hundreds of membrane pores between two mating cells. The pores expand, forming a membrane lattice with wide apertures, allowing cells to exchange gametic nuclei (13). The pores, 100–200 nm in diameter, require a curved localized membrane structure, which energetically favors certain lipids, excluding others (4). The mating process and pore formation can be synchronized such that the majority of the cells will be at the same mating step. Because the domain observed during mating forms without external manipulation, it is possible to determine whether changes in composition precede or follow changes in structure.

Mass spectrometry imaging has been used to observe lipid domains in conjugated single-cell organisms during mating (4). This discovery confirmed that the local composition of the plasma membrane of living cells is intimately related to its localized structure but raised the important question: Does the membrane lipid composition drive its structure or does the structure determine the membrane lipid composition? This is essentially a classic "chicken or the egg?" scenario. One possibility is that the membranes of these cells alter their lipid distribution and possibly their composition prior to fusion, thus anticipating the fusion event. The implication is that the lipid domains may help to drive fusion. Indeed, membrane fusion in *Tetrahymena thermophila* mating is dependent upon both lipid (14) and protein (15) synthesis. Conformational changes called tip transformation, which occur prior to fusion during a period called costimulation, have also been observed at the anterior end of the cells where fusion will eventually take place (15). The motivation to examine these cells at different stages of mating by using mass spectrometry imaging was primed by these findings. The alternate possibility is that the local composition changes to minimize the energy of the bending membrane.

Two scenarios for the process by which lipid domains are formed are depicted in Fig. 1. In this model, we use lysolipids of uncertain headgroup and hexagonal II (H II) lipids to displace the cylindrical lipids, resulting in the observed lipid domain, which either precedes or follows pore formation. The bottom pathway represents domain formation preceding and preparing for membrane fusion. The upper pathway represents domains that are formed in response to the structural changes, fusion, and pore formation. Determining when the local composition changes relative to the fusion event could rectify this difference. In this paper, mating *Tetrahymena* were examined with mass spectrometry imaging to determine if membrane fusion during the mating process creates lipid domains or if the cells have some mechanism, by anticipation of pore formation, to preform lipid domains.

Results

Lipid Domain Formation Correlates with Pore Formation. To investigate when the lipid domain forms relative to fusion, we used time-of-flight secondary ion mass spectrometry (TOF-SIMS) imaging. We have previously established TOF-SIMS imaging with freeze fracture sample preparation as a method to track lipid domain formation (4). Furthermore, images of the phosphocholine (PC) ion (m/z 184), indicative of the lamellar lipids phosphatidylcholine and sphingomyelin, serve as a diagnostic tool to identify *Tetrahymena* mating domains; the PC signal decreases in the area where the two cells have fused (4). This is the only technique currently known to provide the chemical specificity and submicron lateral resolution required to directly visualize such domains (4, 16). In TOF-SIMS the secondary ions are accelerated into a TOF mass spectrometer, separating them by their mass-to-charge

Author contributions: M.E.K., C.T.V.B., and A.G.E. designed research; M.E.K. and P.D.P. performed research; C.T.V.B. and N.W. contributed new reagents/analytic tools; M.E.K., P.D.P., M.L.H., N.W., and A.G.E. analyzed data; and M.E.K., M.L.H., N.W., and A.G.E. wrote the paper.

The authors declare no conflict of interest.

*This Direct Submission article had a prearranged editor.

[1]To whom correspondence should be addressed. E-mail: andrewe@chem.gu.se.

This article contains supporting information online at www.pnas.org/cgi/content/full/0908101107/DCSupplemental.

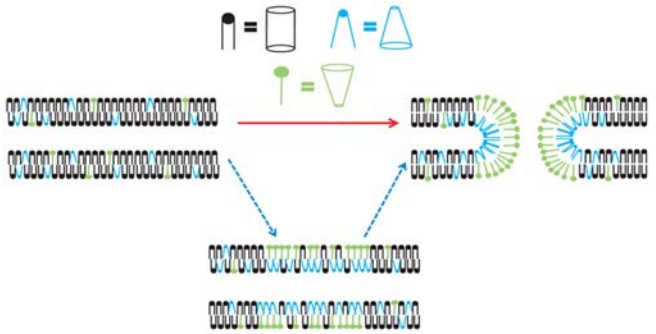

Fig. 1. Schematic of two domain formation scenarios for mated *T. thermophila*. Heterogeneously distributed lipids in the plasma membranes of *T. thermophila* might form as a result of (*Red Arrow*) or in anticipation of pore formation (*Blue Arrows*). Black lipids are cylindrical, blue are H II, and green are lysolipids.

ratio and detecting them. An image is constructed by collecting mass spectra as a function of the position of the primary ion beam as it is raster-scanned across the surface. A mass spectrum is collected at each pixel, spatially revealing the chemical composition of the surface.

In order to establish the link between changes in structure and lipid composition in mated *T. thermophila*, it was important to identify the point at which stable pores had been formed between the two cells. Cell pairs can be described as being either strongly or weakly paired. The distinction is that strongly paired resist separation, which can be brought about by physical perturbation or the addition of exogenous agents to the media (15, 17, 18). This resistance to separation is taken to be evidence for the formation of stable pores (19). Here we use a physical perturbation called trituration to discriminate strongly and weakly paired cells (18) so the pairs known to have formed stable pores could be imaged by using TOF-SIMS.

A differential interference contrast image of paired cells is shown in Fig 2*A*, and SIMS images of a triturated mated pair are shown in Fig. 2*B–D*. The image in Fig. 2*B* maps $C_5H_9^+$ (m/z 69), a hydrocarbon fragment ubiquitous to the acyl chains found in phospholipids (4, 20, 21). This chemical image shows that the membranes of the two cell are in contact because the signal is continuous through the junction. In fact, the membranes are fused, as evidenced by the cells' resistance to separation following trituration. The ion image also serves as an internal standard, which is used to compare ion signals from other molecules from the membrane surface (4, 20, 21). The $C_5H_9^+$ signal is consistent throughout the junction, and thus fluctuations in the lipid signal were taken to reflect changes in concentration across the membrane surface. The image in Fig. 2*C* maps the surface concentration of PC. The most dramatic feature in this image is the lack of signal in the junction of the two cells. This is the previously reported lipid domain (4); however, here by using trituration we have confirmed that pores have formed between the two cells and that they coexist with the lipid domain. The SIMS image in Fig. 2*D* maps m/z 126 the headgroup a diagnostic ion used to identify 2-aminoethylyphosphonolipid (2-AEP) (4). This nonlamellar lipid does not decrease in the junction region like the PC ion. To the contrary, the 2-AEP signal appears more intense in the region lacking the lamellar lipids. Mass spectra taken from two regions of interest, the cell–cell junction and the cell bodies, are shown in Fig. 2*E*. The spectra show the average intensity of the pixels in the regions selected. The spectra show that the PC signal does not appear in the junction, whereas it does in the cell bodies, and that the 2-AEP appears in both regions. Trituration has been used here to isolate paired cells with pores, but it cannot be used to directly isolate weakly paired cells with no pores, because the procedure separates these cells. To investigate weakly paired

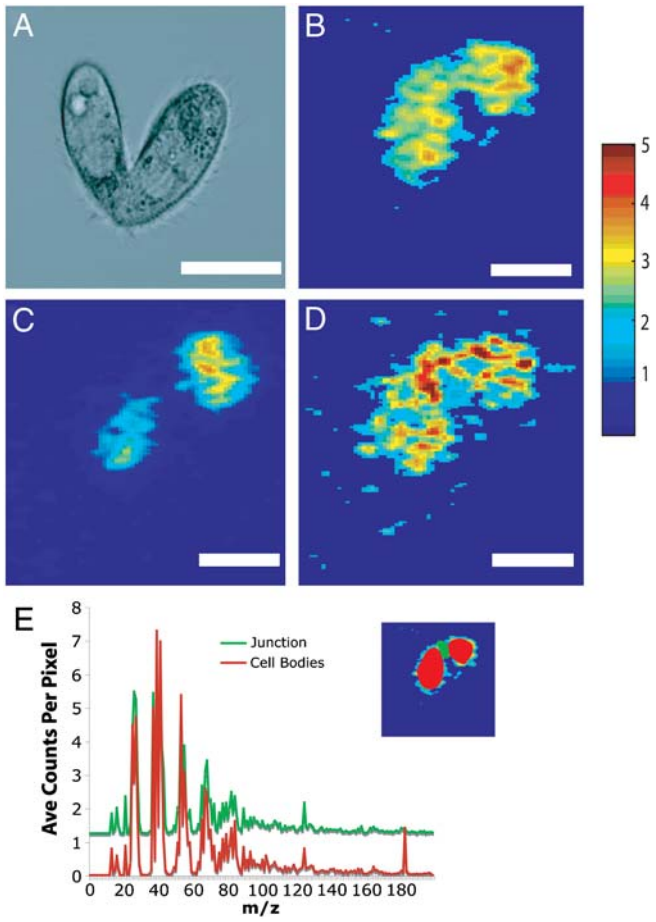

Fig. 2. SIMS analysis of a strongly paired mated *T. thermophila*. (*A*) Differential interference contrast microscopy image of a mating cell pair. (Scale bar: 25 μm.) (*B–D*) SIMS images of a triturated pair of mating *T. thermophila*. C_5H_9 is mapped in (*B*), PC is mapped in (*C*), and 2-AEP is mapped in (*D*) (the intensity in the 2-AEP image has been multiplied by 3). (*E*) Region of interest analysis of the same cells. The red mass spectrum is from the cell bodies, and the green mass spectrum is from the junction. The *Inset* highlights the regions on the SIMS image, red for the cell bodies and green for the junction.

cells, mating *Tetrahymena* had to be analyzed under quiescent conditions.

Trituration Determines Time Scale for Strong Pair Formation. Mating in *Tetrahymena* lasts several hours and can be synchronized such that the total population of cells will advance through the process at roughly the same rate. In an attempt to understand the dynamics of the membrane pores formed during mating, *Tetrahymena* biologists have put together the following sequence: (*i*) starved cells, (*ii*) costimulation (0–30 min for fastest cells) with resulting "tip transformation," (*iii*) loose pairing (30–60 min for fastest cells) with easy disruption by refeeding, agitation, etc., and (*iv*) tight pairing (60 min for fastest cells) with acquisition of resistance to separation by refeeding, agitation, etc. (15, 22–24). When serial sections of loose pairs are examined by electron microscopy, there are no pores connecting loose pairs, only broad flattened surfaces with uniform distance between the two cells. Once tight pairs appear (>1 h), then pores appear. This established sequence and response to agitation was applied to the strains of *T. thermophila* used in this study (B and CU428.1) to experimentally choose time points for analysis that would correspond to cells that were either weakly or strongly paired.

To determine the time scale of domain formation, rapid freezing was used to arrest the mating process, followed by TOF-SIMS analysis. Cells will initiate pairing only in the presence

of complementary mating types; hence we define time zero as the point when the two cell types are mixed. This time point corresponds to the start of the costimulation stage mentioned above. The time scale for pair formation vs. pore formation was determined so that aliquots of weakly paired cells could be extracted, frozen, freeze fractured, and analyzed. Cells were frozen for analysis at several time points and the lipids in the membrane measured and correlated to pair formation and ultimately membrane fusion. Cells were examined at 1 (weakly paired cells), 2 (weak/strong pair intermediates), and 3 h (strongly paired cells). This examination was done by tracking the number of cells that pair under quiescent conditions to the number of cells that stay paired following trituration (Fig. 3). Most cell pairs were formed during the initial hour of mating. These pairs were determined to be weakly paired because at the same time point under trituration conditions no pairs were observed. The transition from weakly paired to mated cells occurred from 90 to 150 min with 50% mated at 120 min following the initiation of the experiment. The plot obtained from the trituration experiment was used to determine the time points when aliquots of the suspension of mating cells would be extracted and frozen. SIMS experiments were then carried out at these time points on cells that had not been triturated.

Domains Form After Strong Pairing. Initial studies with TOF-SIMS imaging of mating *Tetrahymena* were carried out on fully mated cells, demonstrating lipid domains. In that work, cells were analyzed later in the process (several hours) and exhibited distinct lipid domains (4). In this work, mass spectrometry imaging shows that weakly paired cells do not display lipid domains. In addition, no lipid heterogeneity was observed in single cells after the stimulation of mating when imaged with TOF-SIMS whether cells were triturated or quiescent. In the first step following formation of cell pairs (1 h), all the weak pairs analyzed, with the exception of one, did not display a lipid domain in the TOF-SIMS images.

Four different cell pairs are imaged in Fig. 4 with the top panels (Fig. 4*A–D*) showing the total ion images, which show the intensity of all the ions measured at the surface from m/z 0–500 for reference. These data show variation in signal intensity across the surface. This variation may reflect signal fluctuations on the basis of both topography and the local chemical matrix. Normalization of the signal of interest to the total ion signal accounts for these factors so that the signal more accurately represents chemical concentration (25–27). A representative cell pair imaged at 1 h is shown in the first column of Fig. 4. Below the total ion images are raw ion images of PC ($m/184$) in Fig. 4*E* and the ubiquitous hydrocarbon fragment C_5H_9 (m/z 69) in Fig. 4*I*. Each of these images has a line drawn across the cell junction corresponding to the line scans in Fig. 4*M* (details concerning line scans are in *SI Text*). Image pixel intensity was averaged and plotted against distance across each cell and the cell-to-cell junction to provide line scans of relative signal intensity. This method was previously used to identify and measure lipid domains in these cells by Ostrowski et al. (4). At the 1-h time point, the images and the line scans show that there is no decrease in either PC or C_5H_9 signal in the cell junction. To account for topography and matrix effects, the PC signal was normalized to the signal from the total ion (Fig. 4*Q*). The lack of variation in intensity (line scans of normalized images are also provided in *SI Text*) supports the conclusion drawn from the raw line-scan analysis—lipid domains are not present in junctions of weakly paired mated *Tetrahymena*. By using the method previously described, the average magnitude of the signal decrease in the cell junction was calculated to be $9 \pm 9\%$. This value is significantly lower than the reported value of $67 \pm 8\%$ for cells which had been analyzed 4 h after the initiation of costimulation (4). Furthermore, only one of the cells analyzed at this time point displayed a trough at the junction in the line scan that resembled the line scans shown in the work done by Ostrowski et al. However, the magnitude of the decrease was lower ($21 \pm 5\%$) than the lowest value previously reported of $44 \pm 6\%$ (4). The observation of a relatively small lipid domain in a cell at 1 h suggests that this particular cell pair was advancing through the process relatively quickly compared to the rest of the population, as it was stated above that the fastest cells form strong pairs at 60 min. Weakly paired cells are known to be disrupted following treatment with concavolin A, a plant lectin with affinity for glycoproteins on the cell surface (18), suggesting that this initial pairing is dictated by a protein interaction before pores are formed.

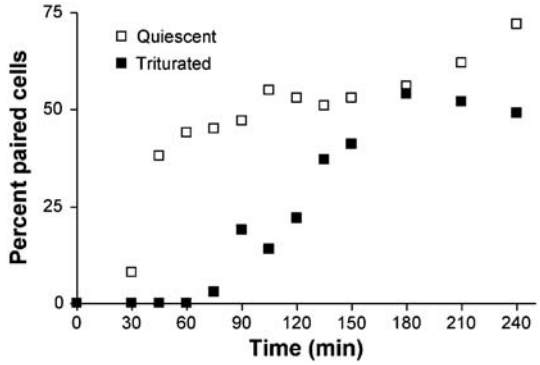

Fig. 3. Pair formation and strong pair formation. The percent of cells paired plotted over time under quiescent conditions and the percent of cells paired following trituration. Pairs resisting trituration are strongly paired.

The second column of Fig. 4 shows the same analyses for one cell pair imaged at 2 h following the initiation of costimulation. The raw PC (Fig. 4*F*) and C_5H_9 (Fig. 4*J*) and the accompanying line scans (Fig. 4*N*) show that this cell pair lacks a discreet signal decrease at the junction of either PC or C_5H_9. Normalization of the PC signal to the total ion signal (Fig. 4*R*) confirms this result by showing a homogenous distribution of PC signal across both cells.

A different cell pair analyzed at 2 h exhibiting a lipid domain is shown in the third column of Fig. 4. The ion image for PC (Fig. 4*G*) shows a drop in intensity at the junction, whereas the C_5H_9 image (Fig. 4*K*) shows a consistent signal across the junction. The line scans for these images (Fig. 4*O*) reveal a trough in the PC signal at the junction and a gradual increase in C_5H_9 signal across the cells, but clearly lacking a trough. The normalized PC image (Fig. 4*S*) corrects for the signal increase across the cells and again shows the signal decrease in the junction region. Line-scan analysis of the images collected at 2 h yielded an average PC signal decrease of $28 \pm 16\%$, and the average decrease in the line scans displaying domains manifested as troughs ($n = 6$) was $38 \pm 15\%$. This observation illustrates two points. First, during the intermediate time point of 2 h there appear to be two populations of cells, one with domains and one without. Second, the PC depletion in cells that exhibit domains at this intermediate stage is not yet to the level of the cells observed at 4 h (4).

The forth column of Fig. 4 contains the analysis of a cell pair 3 h following the initiation of costimulation. The PC ion image (Fig. 4*H*) shows a decrease in PC signal at the cell junction, and the C_5H_9 image (Fig. 4*L*) shows a less dramatic decrease in signal. This result is also apparent in the line scan (Fig. 4*P*). Normalizing the PC signal to the total signal (Fig. 4*T*) has a marked effect on the intensity of the leftmost cell; however, the intensity at the junction is still decreased relative to both cell bodies. The average signal decrease calculated by using the signal intensities from the line scan was $68 \pm 15\%$, in excellent agreement with the previously reported value (4).

Interestingly, the lipid concentration appears to show domain structure across the central surface of these cells as observed in the images. Although this might be extremely exciting, these

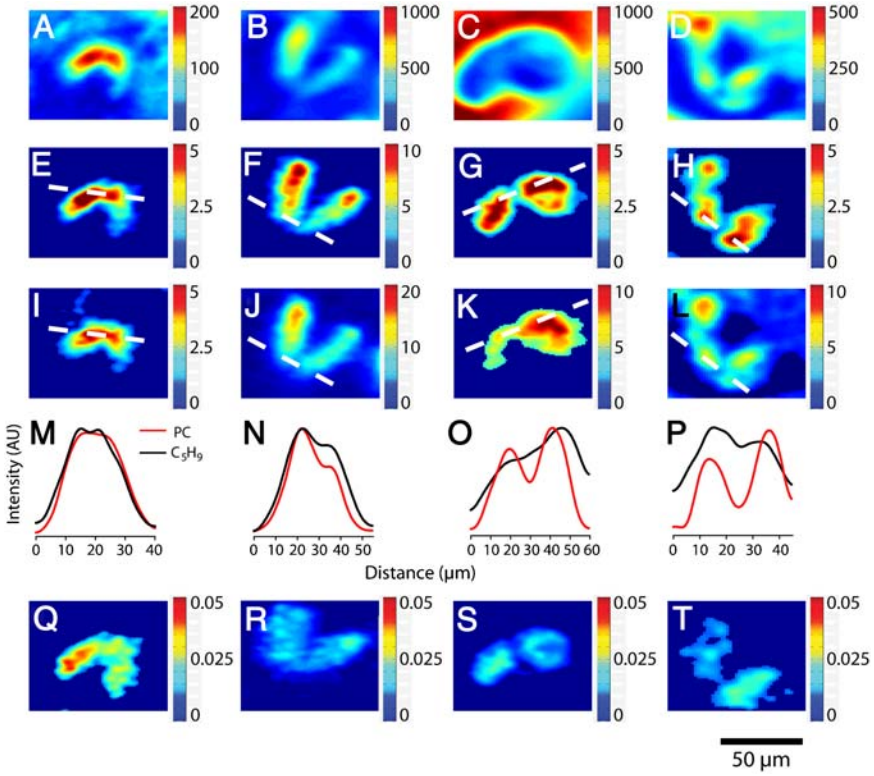

Fig. 4. SIMS images show the temporal evolution of the observed lipid domain formed during cell conjugation. First row: Total ion images of cells imaged at 1 (*A*), 2 (*B* and *C*), and 3 h (*D*). Second row: Phosphatidylcholine ion images (m/z 184) of cells imaged at 1 (*E*), 2 (*F* and *G*), and 3 h (*H*). Third row: C_5H_9 ion images (m/z 69) of cells imaged at 1 (*I*), 2 (*J* and *K*), and 3 h (*L*). Fourth row: Line scans of the ion intensities of phosphatidylcholine and C_5H_9 across the cell–cell junctions for cells imaged at 1 (*M*), 2 (*N* and *O*), and 3 h (*P*). Fifth row: Normalized phosphatidylcholine ion images (m/z 184 divided by total ion) of cells imaged at 1 (*Q*), 2 (*R* and *S*), and 3 h (*T*). The color-coded bars indicate the counts per pixel observed in *A*–*L*, and in *Q*–*T* these show the counts for phosphatidylcholine divided by total counts in each pixel.

variations are not as prominent as those across the junctions of strongly paired cells.

PC Signal Decreases in the Junction over Time. The effects of topography and matrix effects presented by others (25–27) and exhibited by the normalized PC images (Fig. 4*Q*–*T*) show that normalization to total counts is a useful approach to use SIMS imaging to investigate concentrations of surface molecules. Normalization of signals from the region of interest (see *SI Text* for details), however, did not significantly alter the results obtained by using the line-scan method used by Ostrowski et al. (4). Thus the conclusions made are supported by both methods of data analysis. The normalized region of interest analysis of the PC molecular fragment ion for the three regions of the paired cells is shown in Table 1. The PC intensities were normalized to the number of pixels in the region and to the total ion counts per pixel. Table 1 shows that the amount of PC in the junction of mated *Tetrahymena* significantly decreases as cells are mated for longer times (one-way ANOVA, $p < 0.01$). We hypothesize that the evolution of the observed lipid domain depends on changes in the superstructure of the membrane at the cell–cell junction, i.e., pore formation, which require nonlamellar lipids for stability. Additionally, it has been proposed that following initial formation, pores broaden and form a mesh of lipid microtubules (24). By assuming this mechanism for domain formation, Table 1 also suggests that the rate of the structural changes increases over time. Table 1 shows that between 1 and 2 h PC decreases by 22% from 7% to 29% and then by another 40% between 2 and 3 h. The observed increase in the rate of this loss might be because of membrane reorganization caused by the initial events making the membranes more amenable to fusion.

Domain Formation Correlates to Trituration Resistance. We examined the correlation between lipid domain formation and the strength of cell pairing (response to trituration). Cell pairs that did not display a significant trough in the line scan (less than 20% signal decrease in the junction) were defined as not containing lipid domains. The percent of cells displaying domains at each time point is compared to the percent of cells resisting trituration in Fig 5. The pairs analyzed that did not show lipid domains were all from either the 1 or the 2-h time point. Indeed, one-third of the pairs analyzed at the intermediate time of 2 h did not display lipid domains. The appearance of lipid domains correlated well to the resistance of pairs to separate following trituration. Apparently the formation of lipid domains in the cell pairs identifies the threshold from which cell mating cannot be easily disrupted.

Table 1. Summary of normalized (25) PC intensities across mating *T. thermophila* from three regions of interest. Errors are in SD.

Time (h)	Cell body I	Junction	Cell body II	Percent decrease
1 ($n = 6$)	$9.9 \times 10^{-3} \pm 6.7 \times 10^{-3}$	$9.2 \times 10^{-3} \pm 0.67 \times 10^{-3}$	$10.2 \times 10^{-3} \pm 8.1 \times 10^{-3}$	7% ± 15
2 ($n = 9$)	$14 \times 10^{-3} \pm 2.7 \times 10^{-3}$	$9.7 \times 10^{-3} \pm 4.2 \times 10^{-3}$	$14 \times 10^{-3} \pm 3.9 \times 10^{-3}$	29% ± 27
3 ($n = 4$)	$8.6 \times 10^{-3} \pm 7.8 \times 10^{-3}$	$2.7 \times 10^{-3} \pm 2.5 \times 10^{-3}$	$9.3 \times 10^{-3} \pm 6.7 \times 10^{-3}$	69% ± 10

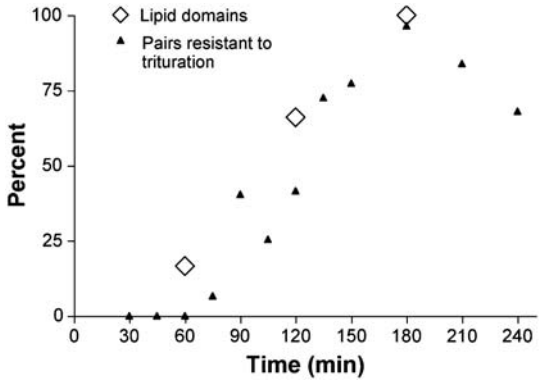

Fig. 5. The percent of paired cells displaying lipid domains over time vs. the percent of paired cells that resisted separation following trituration. Three time points were investigated: 60 ($n = 6$), 120 ($n = 9$), and 180 min ($n = 4$). Domains were defined as a decrease in phosphocholine at the junction between cells (4). Line scans of PC intensity were used to measure this decrease. The appearance of a trough was used to determine that a pair had formed a lipid domain.

Discussion

Membrane pore formation involves significant bending of local membrane structure. During bending, the redistribution of lipid composition has been studied with model membrane systems. Homogenous, flat lipid monolayers were shown to form regions with heterogeneous lipid composition when bent, with the nonlamellar lipid concentrated in the areas of highest curvature (28). Additionally, phase separation of lipids can be induced by constructing a lipid bilayer on a curved surface (29). These phenomena are described by the theory of intrinsic curvature, which states that lipid shape contributes to the spontaneous curvature of the membrane (30). In live cell experiments, degranulation of mast cells was inhibited when the contacting monolayers, i.e., the outer leaflet of the vesicle and the inner leaflet of the plasma membrane, were treated with lysophosphatidylcholine, a micelle-forming lipid (positive intrinsic curvature) (31). In contrast, incubation of isolated chromaffin granules with arachidonic acid (negative intrinsic curvature) promotes fusion (32). Amatore et al. recently showed that these lipids could each produce the opposite effect when added to the extracellular media (the noncontact side of the fusing membranes) of chromaffin cells undergoing exocytosis (33). In a similar experiment PC12 cells were incubated with dipalmitoylphosphatidylcholine, a lamellar lipid (close to no intrinsic curvature), resulting in a decrease in the rate of exocytosis (34). In summary, experiments with model systems show that physical manipulation can be used to redistribute membrane composition, and cell experiments show that altering composition can regulate the dynamics of the fusion event. These results offer conflicting hypotheses; alteration of local lipid composition may be the cause or effect of altered membrane structure. These studies unequivocally show the importance of nonlamellar lipids in forming high curvature regions and fusion of lipid membranes.

Lipid domains observed across the highly curved junction membranes in mated *Tetrahymena* are not observed in single cells prior to mating nor are they observed in significant numbers in weakly paired cells at early times. Hence, the hypothesis that lipid domain formation precedes strong pairing of cells is excluded. Moreover, domains do not form until the cells have become strongly paired. In the sequence of events during *Tetrahymena* mating, the formation of loose to tight pairs of cells occurs between 30 and over 60 min, which correlates to physical changes in the membrane including a change from a flat membrane interface to the formation of pores connecting the cells (15, 22–24). The two SIMS data points shown here at 2 and 3 h correspond with pore-possessing cells and have PC redistribution. The 1-h SIMS point should consist of loosely paired, poreless cells, and according to the model there should be no PC redistribution, as we generally observe. Thus, PC redistribution occurs in the time frame of pore formation, which suggests that the two events are interrelated. Presumably, the PC concentration decreases to make the spontaneous curvature of the contacting layers negative, but this is not a precondition for fusion. It has been shown that the fusion protein synaptotagmin can induce membrane curvature (35); a similar mechanism could be at work here. Protein-induced membrane deformation and pore formation may alter the local membrane composition. As the pores develop and increase in number, more high curvature lipid is recruited to the junction displacing PC. This increase in high curvature lipid produces the observed time-dependent decrease in PC at the junction. Therefore, mass spectrometry images of mating *Tetrahymena* suggest that pore formation drives the formation of lipid domains. Thus, the physical structure, in this case high membrane curvature, needed to support a function dictates composition at this level.

The mechanism by which the cellular machinery constructs highly curved membrane structures is highly important, as dynamic membrane processes are ubiquitous in cell biology. The composition of the cell membrane is continuously being modified via fusion and fission events. Our results suggest that function and structure dictate membrane composition rather than a mechanism where composition is altered in anticipation of function. This membrane composition is clearly important in determining cellular regulating factors, and recent observations have shown that incubation with lipids can alter the rate of chemical release via exocytosis (34, 35). If, indeed, structure dictates the chemical composition of membranes, then it is convenient to speculate that membrane fusion events during exocytosis result in a subsequent change in local membrane composition. The different composition could change further dynamic events by facilitation or inhibition, which in turn would lead to plasticity in the process, could serve numerous functions in the cell, and might be part of the basis of short-term memory.

Material and Methods

Mating *Tetrahymena*. *T. thermophila* strains B and CU428.1 were maintained at room temperature in 0.5% proteose peptone/0.5% tryptone/0.02% K_2HPO_4/0. 01% crude soybean lecithin/0.025% Fe-EDTA and grown at 30 °C in 2% proteose peptone/0.2% yeast extract/0.5% dextrose/0.01% crude soybean lecithin/0.025% Fe-EDTA. Starvation was induced by centrifugation at $200 \times g$ for 4 min, washing with 10 mM Hepes adjusted to pH 7.3 with NaOH. The cells were then resuspended in Hepes at 30 °C and shaken. Cell densities were obtained by microscopic examination of samples fixed and diluted in phosphate-buffered formalin. Cells starved for 16–20 h were mixed to yield a 1:1 ratio of the two strains at a density of approximately 10^6 cells/mL. Aliquots of 2 mL were distributed to wells of Falcon 353046 6-well plates maintained at 30 °C.

Trituration. One milliliter of cell suspension was removed from a 2-mL mating mix with a 1000-μL Eppendorf micropipet and transferred to an empty well in a 6-well plate. The cells were drawn in and out of the pipet 5 times to disrupt weak pairs and then returned to the well. The result is two wells containing 1 mL of cell suspension, one that has been triturated and one that has not. One milliliter of 2.4% glutaraldehyde in 0.2 M sodium phosphate buffer, pH 7.0, was then added to both the triturated and undisturbed mating mixes.

Cell Counting. Cells were counted at several time points over a 4-h period during mating: 0 min, 30 min, then every 15 min until 210 min, and 240 min. Aliquots were taken from the mating cell suspension and fixed in a formalin solution to terminate the

mating process. Aliquots were taken twice for each time step. One aliquot was triturated whereas the control cells were left undisturbed until fixation. Single and paired cells were counted and the percent of cells paired was determined. A minimum of 300 fixed cells was examined as described by Van Bell and Williams (17). The percent of paired cells resistant to trituration was determined by dividing the percent of paired control cells by the percent of paired cells following trituration.

SIMS Imaging. Cells were prepared for analysis in vacuum by using a freeze fracture procedure for SIMS imaging described previously (36). Cells were imaged at three time points; 1, 2, and 3 h following mixing of the two mating types. SIMS imaging was carried out by using a Kratos Prism TOF-SIMS spectrometer equipped with a 15-kV FEI indium liquid metal ion source, was focused to a beam size of approximately 500 nm, and delivered 1 nA of current to the sample at 45° with 50-ns unbunched pulses at a repetition rate of 1.5 kHz. The sample was mounted onto a LN_2-cooled analysis stage (Kore Tech. Ltd.). The mass resolution for these experiments was $m/\Delta m$ 500 (detail provided in *SI Text*).

SIMS imaging was performed by electrostatically raster-scanning the primary ion beam across the sample and collecting a mass spectrum at every pixel in either the 128×128 pixel image in a 102×138 μm field of view or 256×256 in the 146×197 μm field of view. Molecular ion images were generated by selecting a mass of interest from the total ion mass spectrum and plotting the intensity at each pixel. Image processing, including normalization to the total ion signal, a two-dimensional smooth, and signal thresholding, was done in MATLAB (MathWorks, Inc.).

ACKNOWLEDGMENTS. This work was supported by National Institutes of Health Grant 2R01EB002016-16 (to N.W. and A.G.E). A.G.E. is supported as a Marie Curie Chair from the European Union 6th Framework.

1. Chernomordik LV, Zimmerberg J, Kozlov MM (2006) Membranes of the world unite!. *J Cell Biol* 175(2):201–207.
2. Blumenthal R, Clague MJ, Durell SR, Epand RM (2003) Membrane fusion. *Chem Rev* 103(1):53–69.
3. Yang L, Huang HW (2002) Observation of a membrane fusion intermediate structure. *Science* 297(5588):1877–1879.
4. Ostrowski SG, Van Bell CT, Winograd N, Ewing AG (2004) Mass spectrometric imaging of highly curved membranes during Tetrahymena mating. *Science* 305(5680):71–73.
5. Simons K, Ikonen E (1997) Functional rafts in cell membranes. *Nature* 387 (6633):569–572.
6. Hao MM, Mukherjee S, Maxfield FR (2001) Cholesterol depletion induces large scale domain segregation in living cell membranes. *Proc Natl Acad Sci USA* 98(23):13072–13077.
7. Edidin M (2001) Shrinking patches and slippery rafts: Scales of domains in the plasma membrane. *Trends Cell Biol* 11(12):492–496.
8. Maxfield F (2005) Role of cholesterol and lipid organization in disease. *Nature* 438 (7068):612–621.
9. Scherzer CR, Feany MB (2004) Yeast genetics targets lipids in Parkinson's disease. *Trends Genet* 20(7):273–277.
10. Cutler RG, et al. (2004) Involvement of oxidative stress-induced abnormalities in ceramide and cholesterol metabolism in brain aging and Alzheimer's disease. *Proc Natl Acad Sci USA* 101(7):2070–2075.
11. Mattson MP, Cutler RG, Pedersen WA (2002) Perturbed sphingomyelin metabolism and accumulation of ceramides and cholesterol esters in Alzheimer's disease and ALS. *J Neurochem* 81:60–63.
12. Escriba PV (2006) Membrane-lipid therapy: A new approach in molecular medicine. *Trends Mol Med* 12(1):34–43.
13. Orias JD, Hamilton EP, Orias E (1983) A microtubule meshwork associated with gametic pronucleus transfer across a cell-cell junction. *Science* 222(4620):181–184.
14. Frisch A, Loyter A, Levy R, Goldberg I (1978) Inhibition of conjugation in Tetrahymena pyriformis by cerulenin. Possible requirement for de novo lipid synthesis. *Biochim Biophys Acta* 506(1):18–29.
15. Wolfe J (1982) The conjugation junction of Tetrahymena: Its structure and development. *J Morphol* 172:159–178.
16. Kraft ML, Weber PK, Longo ML, Hutcheon ID, Boxer SG (2006) Phase separation of lipid membranes analyzed with high-resolution secondary ion mass spectrometry. *Science* 313(5795):1948–1951.
17. Van Bell CT, Williams NE (1984) Membrane-protein differences correlated with the development of mating competence in Tetrahymena-thermophila. *J Protozool* 31(1):112–116.
18. Ofer L, Levkovitz H, Loyter A (1976) Conjugation in Tetrahymena-pyriformis—Effect of polylysine, concanavalin-a, and bivalent metals on conjugation process. *J Cell Biol* 70(2):287–293.
19. Allewell NM, Oles J, Wolfe J (1976) Physicochemical analysis of conjugation in Tetrahymena-pyriformis. *Exp Cell Res* 97(2):394–405.
20. Ostrowski SG, Kurczy ME, Roddy TP, Winograd N, Ewing AG (2007) Secondary ion MS imaging to relatively quantify cholesterol in the membranes of individual cells from differentially treated populations. *Anal Chem* 79(10):3554–3560.
21. Monroe EB, Jurchen JC, Lee J, Rubakhin SS, Sweedler JV (2005) Vitamin E imaging and localization in the neuronal membrane. *J Am Chem Soc* 127(35):12152–12153.
22. Nelsen EM, Williams NE, Yi H, Knaak J, Frankel J (1994) "Fenestrin" and conjugation in Tetrahymena thermophila. *J Eukaryot Microbiol* 41(5):483–495.
23. Suganuma Y, Shimode C, Yamamoto H (1984) Conjugation in Tetrahymena: Formation of a special junction area for conjugation during the co-stimulation period. *J Electron Microsc* 33(1):10–18.
24. Cole ES (2006) *Cell-Cell Channels* (Landes Bioscience, Georgetown, TX).
25. Rangarajan S, Tyler BJ (2006) Topography in secondary ion mass spectroscopy images. *J Vac Sci Technol A* 24(5):1730–1736.
26. Tyler BJ, Rayal G, Castner DG (2007) Multivariate analysis strategies for processing ToF-SIMS images of biomaterials. *Biomaterials* 28(15):2412–2423.
27. Fletcher JS, Lockyer NP, Vaidyanathan S, Vickerman JC (2007) TOF-SIMS 3D biomolecular imaging of Xenopus laevis oocytes using buckminsterfullerene (C-60) primary ions. *Anal Chem* 79(6):2199–2206.
28. Ding L, et al. (2005) Distorted hexagonal phase studied by neutron diffraction: Lipid components demixed in a bent monolayer. *Langmuir* 21(1):203–210.
29. Parthasarathy R, Yu CH, Groves JT (2006) Curvature-modulated phase separation in lipid bilayer membranes. *Langmuir* 22(11):5095–5099.
30. Gruner SM (1985) Intrinsic curvature hypothesis for biomembrane lipid-composition—A role for nonbilayer lipids. *Proc Natl Acad Sci USA* 82(11):3665–3669.
31. Chernomordik LV, et al. (1993) Lysolipids reversibly inhibit Ca-2+-dependent, Gtp-dependent and Ph-dependent fusion of biological-membranes. *FEBS Lett* 318(1): 71–76.
32. Creutz CE (1981) Cis-unsaturated fatty-acids induce the fusion of chromaffin granules aggregated by synexin. *J Cell Biol* 91(1):247–256.
33. Amatore C, et al. (2006) Regulation of exocytosis in chromaffin cells by trans-insertion of lysophosphatidylcholine and arachidonic acid into the outer leaflet of the cell membrane. *ChemBioChem* 7(12):1998–2003.
34. Uchiyama Y, Maxson MM, Sawada T, Nakano A, Ewing AG (2007) Phospholipid mediated plasticity in exocytosis observed in PC12 cells. *Brain Res* 1151:46–54.
35. Martens S, Kozlov MM, McMahon HT (2007) How synaptotagmin promotes membrane fusion. *Science* 316(5828):1205–1208.
36. Cannon DM, Pacholski ML, Winograd N, Ewing AG (2000) Molecule specific imaging of freeze-fractured, frozen-hydrated model membrane systems using mass spectrometry. *J Am Chem Soc* 122(4):603–610.